How to cite: *Angew. Chem. Int. Ed.* **2021**, *60*, 11847–11851
International Edition: doi.org/10.1002/anie.202103147
German Edition: doi.org/10.1002/ange.202103147

Hydrogels

Recombinant Spider Silk Gels Derived from Aqueous–Organic Solvents as Depots for Drugs

*Vanessa J. Neubauer, Vanessa T. Trossmann, Sofia Jacobi, Annika Döbl, and Thomas Scheibel**

Abstract: *Hydrogels are widely used in various biomedical applications, as they cannot only serve as materials for biofabrication but also as depots for the administration of drugs. However, the possibilities of formulation of water-insoluble drugs in hydrogels are rather limited. Herein, we assembled recombinant spider silk gels using a new processing route with aqueous–organic co-solvents, and the properties of these gels could be controlled by the choice of the co-solvent. The presence of the organic co-solvent further enabled the incorporation of hydrophobic drugs as exemplarily shown for 6-mercaptopurine. The developed gels showed shear-thinning behaviour and could be easily injected to serve, for example, as drug depots, and they could even be 3D printed to serve as scaffolds for biofabrication. With this new processing route, the formulation of water-insoluble drugs in spider silk-based depots is possible, circumventing common pharmaceutical solubility issues.*

Hydrogels are used for biomedical applications such as tissue engineering, drug delivery, and recently also biofabrication.[1] Besides polysaccharides, such as alginate[2] or chitosan,[3] proteins such as *Bombyx mori* silkworm silk[4] or gelatine[5] have been processed into hydrogels using various methods. Also, hydrogel formation of the recombinant spider silk protein eADF4(C16), which is engineered based on the repetitive core domain of one of the *Araneus diadematus* dragline silk proteins,[6] has been investigated thoroughly.[7] Spider silk hydrogels exhibit shear-thinning behaviour,[7a] which is a crucial requirement for 3D printing and biofabrication[8] or the administration as drug depots.[9] Modifications during processing allowed incorporating water-soluble biologicals in eADF4(C16) hydrogels and their sustained release.[9] However, several pharmaceutical active agents show only poor water solubility or stability and cannot be delivered using hydrogels. Therefore, the aim of this study was to provide drug depots based on gels with the possibility to formulate both water-soluble and water-insoluble drugs.

Ions such as potassium or phosphate effect folding[10] of spider silk proteins,[11] and this kosmotropic ion-triggered structure formation is part of the natural assembly process of spider silk.[12] However, protein folding effects can be also achieved using non-physiological organic co-solvents when they are fully miscible in water.[13] The presence of organic co-solvents with varying polarity can change the solvation conditions, often leading to protein conformational changes.[13] The assumption that especially hydrophobic interactions and hydrogen bonds are driving forces of protein folding is commonly agreed with.[14] Besides intramolecular folding, also intermolecular structure formation can be obtained in aqueous–organic solvents yielding protein assembly and fibrillisation.[15]

Therefore, we investigated a novel gelation route of recombinant spider silk proteins upon fibril assembly in aqueous–organic micro-heterogeneous phases, including the underlying assembly mechanism, and we provide evidence for the use of gels made therewith as drug depots as well as their 3D printability.

Recombinant spider silk proteins have previously been reported to assemble into fibrils and/or particles upon addition of potassium phosphate, and the gained morphology depends on the concentration of the kosmotropic salt.[6,11,16] Here, we investigated assembly in the presence of co-solvents and -solutes such as DMSO and potassium phosphate and obtained characteristic fibrillisation-based sigmoidal turbidity curves[7a] (Figure 1 A). In order to gain more mechanistic insights into this behaviour, three spider silk protein variants differing in their net charge but with otherwise identical amino acid compositions were analysed (see Experimental Section). Potassium phosphate induced fibrillisation of the negatively charged eADF4(C16),[6] which was used as positive control, and its mechanism of fibrillisation has been reported previously.[11] The positively charged eADF4(κ16)[17] showed accelerated protein aggregation and phase separation in the

[*] V. J. Neubauer, V. T. Trossmann, S. Jacobi, A. Döbl, Prof. T. Scheibel
Lehrstuhl Biomaterialien, Universität Bayreuth
Prof.-Rüdiger-Bormann Strasse 1, 95447 Bayreuth (Germany)
Prof. T. Scheibel
Bayreuther Zentrum für Kolloide und Grenzflächen (BZKG)
Universität Bayreuth
Universitätsstrasse 30, 95440 Bayreuth (Germany),
and
Bayerisches Polymerinstitut (BPI)
Universität Bayreuth
Universitätsstrasse 30, 95440 Bayreuth (Germany),
and
Bayreuther Zentrum für Molekulare Biowissenschaften (BZMB)
Universität Bayreuth
Universitätsstrasse 30, 95440 Bayreuth (Germany),
and
Bayreuther Materialzentrum (BayMAT)
Universität Bayreuth
Universitätsstrasse 30, 95440 Bayreuth (Germany)
E-mail: thomas.scheibel@bm.uni-bayreuth.de
Supporting information and the ORCID identification number(s) for the author(s) of this article can be found under: https://doi.org/10.1002/anie.202103147.

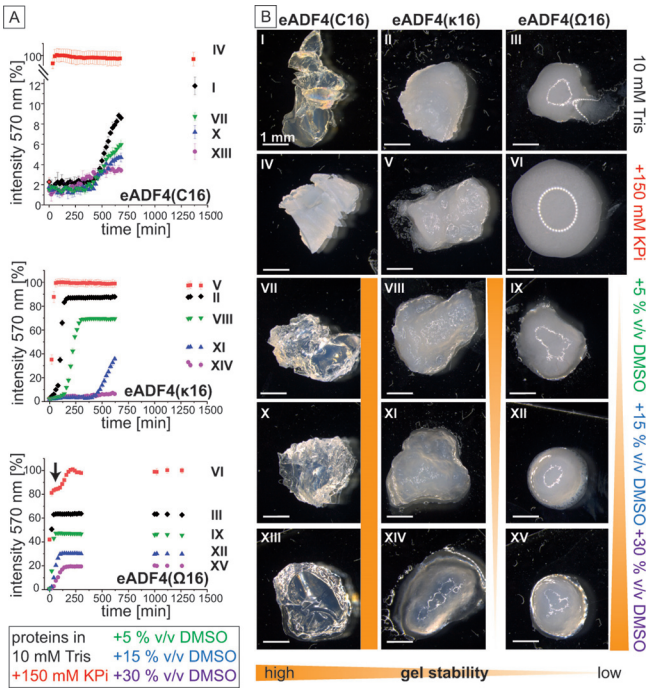

Figure 1. Assembly of three eADF4 variants in presence of different Tris/DMSO volume ratios in comparison to that in presence of 150 mM potassium phosphate (KPi). I–III in 10 mM Tris pH 7.5, IV–VI in presence of 150 mM KPi, VII–IX in presence of 5% (v/v) DMSO, X–XII in presence of 15% (v/v) DMSO, and XIII–XV in presence of 30% (v/v) DMSO. A) Turbidity measurements of eADF4(C16), eADF4(κ16), and eADF4(Ω16) as indicated during fibril formation. Fibril assembly is normalised to KPi samples. The arrow indicates particle formation in case of eADF4(Ω16). B) Stereomicroscopic images of gels at conditions as indicated; scale bars 1 mm. Image VI shows reflections of the light source appearing as a ring. Qualitative gel stabilities are indicated by stability bars.

presence of potassium phosphate, and the uncharged eADF4(Ω16)[18] showed particle formation, indicating a shift towards lower critical potassium phosphate concentrations for particle formation for this variant. The impact of DMSO was analysed in aqueous–organic binary mixtures[19] with different volumes. Like in potassium phosphate, in DMSO the uncharged variant showed the fastest nucleation and fibril growth based on its low electrostatic repulsion, which was least controllable. The positively charged variant showed a fast turbidity increase assuming an aggregation-driven process, yielding gelly morphologies, but no stable gels. The negative variant exhibited the longest lag-phase and yielded well-controllable gels. As this protein is based on the naturally occurring spider silk consensus sequence, the best-controlled assembly behaviour was expected. It has to be mentioned that the addition of DMSO yielded decreased turbidity for all variants and additionally slowed down fibrillisation for eADF4(Ω16) and extended the lag-phase for eADF4(κ16).

Interestingly, gel stability was dependent on both the net charge of the eADF4 variant, as already mentioned above, and the organic additive (Figure 1B), indicating charge-dependent intra- and intermolecular structure formation, as the variants differed in only one amino acid per module in the repetitive sequence. Hydrogen bonds between DMSO and glutamic acid residues within eADF4(C16) were likely the reason for higher gel stability but were independent of the DMSO concentration. In contrast, DMSO seemed to stabilise eADF4(Ω16) gels with increasing concentration, based on hydrogen bonds with glutamine residues. The stability of eADF4(κ16) gelly morphologies decreased with increasing concentration of DMSO, which forms fewer hydrogen bonds with lysine residues.

To investigate the influence of solvent polarity, 3% (w/v) eADF4(C16) solutions, as the best controllable ones, were used in water, and in blends with less polar DMF and with least polar DMSO. Additionally, to gradually increase the concentration of DMSO, 3% (w/v) eADF4(C16) solutions were dialysed against this solvent. The organo-dialysis step allowed a fast solvent exchange and simultaneously lead to highly transparent gels. The effect on protein structure formation was analysed using ATR-FTIR spectroscopy. Secondary structures in gels were derived from the peaks of the amide I and II bands at 1720–1490 cm^{-1} (Figure 2A) and were quantified using Fourier self-deconvolution.

The highest β-sheet content (39 ± 1%) was found in case of Tris-hydrogels as well as gels made in DMSO blends. Tris/DMSO-gels from organo-dialysis showed a lower β-sheet content of 28 ± 5%, which might be caused by faster gelation.

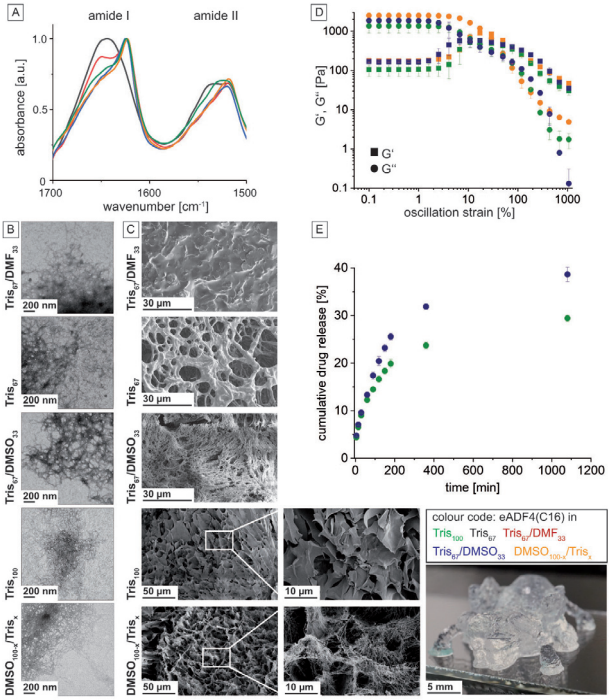

Figure 2. Impact of organic additives on spider silk gels: Comparison of gels from initial 3% (w/v) eADF4(C16) silk solutions in 10 mM Tris pH 7.5 ($Tris_{100}$) diluted with one third volume ratio of the co-solvents water ($Tris_{67}$), DMF ($Tris_{67}/DMF_{33}$), or DMSO ($Tris_{67}/DMSO_{33}$), and gels made upon dialysis against DMSO ($DMSO_{100-x}/Tris_x$). A) Mean ATR-FTIR spectra of the co-solvent gels. B) TEM images of silk fibrils in the co-solvent gels. C) SEM images of the respective co-solvent gels after freeze-drying. D) Mean amplitude sweep rheological measurements of co-solvent gels. E) Normalised cumulative release of 6-mercaptopurine from 2% (w/v) eADF4(C16) $Tris_{100}$ gel (green data points) and from 2% (w/v) eADF4(C16) $Tris_{67}/DMSO_{33}$ gel (blue data points) at 37°C. F) Photo of a 3D printed tarantula from DMSO blend gels ($Tris_{67}/DMSO_{33}$). Scale bar as indicated.

Far fewer β-sheets were found in the presence of water (24 ± 5 %) or in case of blends with DMF (22 ± 4 %). The formation of fibrillar networks was pronounced in the presence of DMSO, indicated by intertwined fibrils as found in TEM images (Figure 2B). In presence of DMF or water, significantly shorter fibrils were formed. SEM imaging showed a sheet-like structure for lyophilised co-solvent gels with DMF. Fused pore structures were found upon water addition. Strikingly, a highly fibrillary and porous structure was present in case of DMSO-triggered gelation. At higher magnification, pore walls showed fibrillar sub-structures in Tris/DMSO-gels after organo-dialysis (Figure 2C). Sharp pore structures were found in Tris-gels with smooth, sheet-like pores as reported previously.[7a] Fibrils in Tris-hydrogels might have collapsed into these sheet structures upon freeze-drying. Rheological characterisation (Figure 2D) showed slightly higher storage and loss moduli for 2 % (w/v) eADF4(C16) Tris/DMSO-gels in comparison to 3 % (w/v) eADF4(C16) Tris-hydrogels. Nonetheless, for Tris/DMSO-gels and Tris-hydrogels, moduli were in the same range, and similar yield points were detected, indicating comparable visco-elastic properties. 3 % (w/v) eADF4(C16) Tris/DMSO-gels from organo-dialysis showed the highest storage modulus and a slight shift in the yield point towards higher oscillation strain, indicating higher resistance of the material until break.

Nonetheless, the new gels showed typical spider silk hydrogel shear-thinning behaviour and stability (Figure S1A,B). Accordingly, using a RegenHU bioplotter, multilayer scaffolds with high shape stability could be 3D printed using the DMSO blend gels (Figure 2F, Figure S3, and Video S4).

To test the application of such gels as drug depots, fluorescein (FITC) was loaded as a first model substance into Tris/DMSO-gels, and a comparison was made to Tris-hydrogels regarding loading and release at 37 °C. Both gel types showed the same release profile (Figure S2), indicating the possibility of generating injectable or transdermal drug-loaded gel depots. Further, the poorly water-soluble 6-mercaptopurine, as clinically relevant cytostatic drug, was loaded into the DMSO-phase of 2 % (w/v) eADF4(C16) blend gels. The drug was incorporated by non-covalent interactions, but in case a reversible coupling is intended, a recently published system with a different spider silk variant can be used.[20] Upon non-covalent introduction in Tris-hydrogels, the water-insoluble drug aggregated during the gelation process and accumulated at the bottom of the gel. In the DMSO blend gel, however, loading and release could be accomplished. These results confirmed the suitability of co-solvent-produced spider silk gels with clinically relevant substances as injectable and even 3D printable drug depots.

Finally, we wanted to unravel the driving force of spider silk assembly in presence of co-solvents. The herein reported route towards spider silk gel formation in aqueous–organic binary mixtures is driven in part by structure formation at organic–water interfaces (Scheme 1). eADF4(C16) was found to form water-insoluble β-sheet structures in microcapsules[21] with barrier function[22] upon adsorption at aqueous–organic interfaces. In case of aqueous–organic binary mixtures, micro-

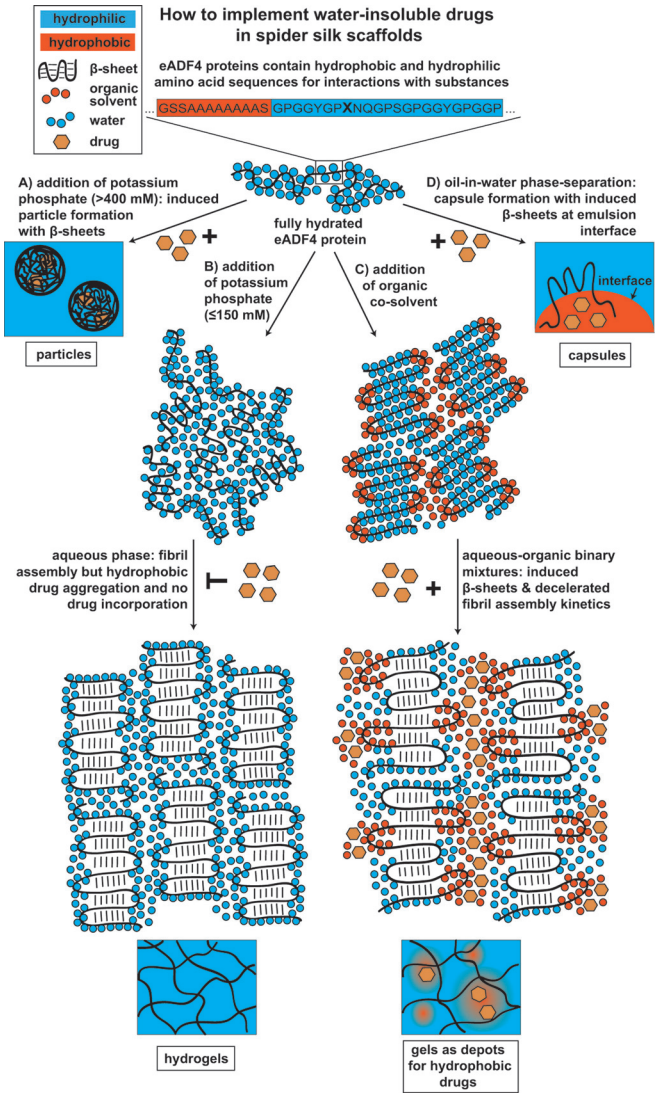

Scheme 1. Illustration of routes towards drug depots made of recombinant spider silk proteins. A) Potassium phosphate-induced co-precipitation of microparticles and any type of drugs. B) Hydrogels cannot incorporate hydrophobic but only hydrophilic drugs during gelation. C) New route of gel formation, allowing the incorporation of hydrophilic as well as hydrophobic drugs. D) Microcapsules can incorporate hydrophilic, hydrophobic, and amphiphilic (at the aqueous–organic interface) drugs. Aqueous–organic binary mixtures as seen in (C) represent intermediate conditions between hydrogel formation in one homogenous (aqueous) phase (B) and phase-separation-induced β-sheet formation at the water–oil interface (D). **X** = selected amino acids of the silk variants, that is, glutamic acid, glutamine, or lysine.

emulsions can form in presence of organic co-solvents such as DMSO[23] or DMF,[13] which are miscible in water.

The formed interphases are micro-heterogeneous[24] and are based on the interaction of hydrogen bond[25] forming molecules. These interphases can be described by a side-by-side arrangement of both solvents in molecular clusters.[25] DMSO and DMF are amphiphilic molecules, which can form hydrogen bonds, for example, with water but also enable hydrophobic interactions among them or with other molecules such as proteins. Similarly, eADF4 exhibits amphiphilic properties due to its amino acid sequence[26] and can therefore

interact with hydrophobic as well as hydrophilic drugs/molecules. Charged amino acid residues can form hydrogen bonds with DMSO to a varying degree, and negatively charged molecules are favoured over uncharged or positively charged ones.[27]

Spider silk gels made out of aqueous–organic co-solvents enlarge the range of applications of spider silk-based materials since material properties can be controlled by the choice of the co-solvent and of the used spider silk variant. DMSO is FDA approved[28] in topical formulations at concentrations at approximately 30 % (v/v). Based on our results it can be applied in spider silk gels in pharmaceutical formulations, e.g. for transdermal applications. These gels allow formulation of water-insoluble drugs along with adjustable organic content to yield biocompatible, biodegradable, non-toxic, non-inflammatory, transdermal, injectable, and even 3D printable drug depots. Depending on the application, the drug–silk interaction can be further controlled, for example, by reversible covalent bonds.[20]

Experimental Section

The engineered spider silk protein eADF4(C16) comprises 16 repeats of the consensus sequence GSSAAAAAAAASGPGGYGPENQGPSGPGGYGPGGP (named C-module). The C-module is based on the consensus sequence of the repetitive core domain of the MaSp2 dragline silk fibroin 4 of the European garden spider *Araneus diadematus*.[6] eADF4(C16) was purchased from AMSilk GmbH (Planegg, Germany). In variant eADF4(κ16),[17] all glutamic acid residues are substituted with lysine and in eADF4(Ω16)[18a] with glutamine ones. Both proteins were produced and purified as reported earlier.[6,17,18] Spider silk proteins were dissolved in 6 M guanidinium thiocyanate (Carl Roth, Karlsruhe, Germany) and dialysed against 10 mM Tris buffer, pH 7.5 for several hours, whereas the dialysis of eADF4(Ω16) was done at 4 °C. Concentration adjustment was conducted, if necessary, by follow-up dialysis in 20 % (w/v) poly(ethylene glycol) (PEG, 20 kDa, Carl Roth, Karlsruhe, Germany) as reported previously[7a] or using a high vacuum concentrator (Speedvac, Eppendorf). For biphasic gels, co-solvents or co-solute buffers were blended with 3 % (w/v) silk solutions and gelled at 37 °C. For organo-dialysis gels, 3 % (w/v) silk solutions were dialysed against small volumes (1:100 volume ratio) of DMSO (Carl Roth, Karlsruhe, Germany) at RT for 4 h without further thermal treatment.

For analysis of the gelation kinetics of recombinant spider silk proteins, turbidity changes were monitored at 570 nm using a microplate reader (Mithras LB 940, Berthold Technologies, Germany). Triplicates of 100 µL aliquots were prepared for all solutions (3 % (w/v) eADF4(C16), 2 % (w/v) eADF4(κ16), and 1 % (w/v) eADF4(Ω16)). Spider silk solutions were diluted by addition of different volumes of DMSO to reach final concentrations of 5, 15, and 30 % (v/v) DMSO in the blend. As a control, 150 mM potassium phosphate was used as fibrillisation trigger, and data were normalised to this sample's endpoint.

Gel samples were transferred on glass slides for image collection using a Leica M205C stereomicroscope (Wetzlar, Germany) with Leica LAS software and light reflection from dark field mode. The microscope was equipped with a polarisation lens and a 0.63× objective. For scanning electron microscopy (SEM), lyophilised gel samples were investigated after platinum sputtering (2 nm). Images were recorded using a Thermo Scientific (FEI) Apreo VS with a Field Emission Gun at 2 kV and a SE2-detector. Transmission electron microscopy (TEM) images of stained (2 % uranyl acetate) spider silk fibrils immobilised on Pioloform-coated 100-mesh copper grids (Plano GmbH, Germany) were recorded using a JEM-2100 TEM (JEOL, Japan), operated at 80 kV, and imaging was carried out using a 4000 × 4000 charge-coupled device camera (UltraScan 4000, Gatan, USA) and Gatan Digital Micrograph software (version 1.83.842).

Rheological behaviour was investigated using a Discovery Hybrid Rheometer 3 (TA, USA) with a plate–plate geometry (diameter 25 mm) at 25 °C. To prevent drying effects on the gels, a wet sponge adapter was used. Amplitude sweeps ($n = 3$) were recorded as triplicates at 31.4 rad s^{-1} and a strain of 0.1–1000 %.

Attenuated total reflectance-Fourier transformation infrared spectroscopy (ATR-FTIR) was conducted with lyophilised gel samples. Spectra ($n = 3$) were recorded using a Bruker Tensor 27 (Ettlingen, Germany) with a germanium crystal at a spectral resolution of 2 cm^{-1} with 100 scans. Atmospheric compensation algorithm was applied in OPUS 8.0 software to correct water vapour and carbon dioxide fluctuations during the measurement. Fourier self-deconvolution was carried out as reported previously[29] with band assignment for partial secondary structure determination.[30]

To study the release of 6-mercaptopurine (Sigma, USA) from 2 % (w/v) $Tris_{100}$ and 2 % (w/v) $Tris_{67}$/$DMSO_{33}$ eADF4(C16) gels, the drug was dissolved in 20 µL DMSO and added to the spider silk solutions or the DMSO-phase. Triplicate release measurements were conducted in 1:1 blends of MilliQ water:DMSO. UV absorbance was monitored using a UV spectrometer (Genesys 10S UV/Vis, Thermo Scientific). Spectra were recorded between 200 and 600 nm, and peak maxima at 328 nm were used to determine cumulative release curves.

3D dispense plotting was carried out using a RegenHU 3D Discovery Gen1 (Switzerland) bioplotter with cartridges size 3cc and according pistons. The printing speed was pre-set to 10 mm s^{-1}. 2 % (w/v) $Tris_{67}$/$DMSO_{33}$ eADF4(C16) gels were printed with Luer lock plastic needles with an inner diameter of 0.41 mm and an applied pressure of 0.3 bar.

Acknowledgements

The authors acknowledge the funding from the Deutsche Forschungsgemeinschaft (DFG, German Research Foundation)—project number 326998133-TRR225 (funded subproject: C01 TS) and SCHE603/24-1. The authors thank Anika Winkler for transmission electron microscopy and Hendrik Bargel for scanning electron microscopy. Open access funding enabled and organized by Projekt DEAL.

Conflict of interest

TS is founder and share-holder of AMSilk GmbH.

Keywords: binary mixtures · co-solvent · hydrophobic effect · micro-heterogeneity · self-assembly

[1] J. L. Drury, D. J. Mooney, *Biomaterials* **2003**, *24*, 4337 – 4351.
[2] a) W.-H. Tan, S. Takeuchi, *Adv. Mater.* **2007**, *19*, 2696 – 2701; b) A. G. Tabriz, M. A. Hermida, N. R. Leslie, W. Shu, *Biofabrication* **2015**, *7*, 045012.
[3] a) N. Bhattarai, J. Gunn, M. Zhang, *Adv. Drug Delivery Rev.* **2010**, *62*, 83 – 99; b) Y. Hong, H. Song, Y. Gong, Z. Mao, C. Gao, J. Shen, *Acta Biomater.* **2007**, *3*, 23 – 31.
[4] N. Wu, H. Yu, M. Sun, Z. Li, F. Zhao, Y. Ao, H. Chen, *ACS Appl. Biol. Mater.* **2020**, *3*, 721 – 734.
[5] T. Zehnder, B. Sarker, A. R. Boccaccini, R. Detsch, *Biofabrication* **2015**, *7*, 025001.
[6] D. Huemmerich, C. W. Helsen, S. Quedzuweit, J. Oschmann, R. Rudolph, T. Scheibel, *Biochemistry* **2004**, *43*, 13604 – 13612.

[7] a) K. Schacht, T. Scheibel, *Biomacromolecules* **2011**, *12*, 2488 – 2495; b) E. DeSimone, K. Schacht, T. Scheibel, *Mater. Lett.* **2016**, *183*, 101 – 104; c) E. DeSimone, K. Schacht, T. Jüngst, J. Groll, T. Scheibel, *Pure Appl. Chem.* **2015**, *87*, 737 – 749.
[8] a) K. Schacht, T. Juengst, M. Schweinlin, A. Ewald, J. Groll, T. Scheibel, *Angew. Chem. Int. Ed.* **2015**, *54*, 2816 – 2820; *Angew. Chem.* **2015**, *127*, 2858 – 2862; b) E. DeSimone, K. Schacht, A. Pellert, T. Scheibel, *Biofabrication* **2017**, *9*, 044104.
[9] S. Kumari, H. Bargel, M. U. Anby, D. Lafargue, T. Scheibel, *ACS Biomater. Sci. Eng.* **2018**, *4*, 1750 – 1759.
[10] F. Hofmeister, *Arch. Exp. Pathol. Pharmakol.* **1888**, *24*, 247 – 260.
[11] U. K. Slotta, S. Rammensee, S. Gorb, T. Scheibel, *Angew. Chem. Int. Ed.* **2008**, *47*, 4592 – 4594; *Angew. Chem.* **2008**, *120*, 4668 – 4670.
[12] a) L. Eisoldt, A. Smith, T. Scheibel, *Mater. Today* **2011**, *14*, 80 – 86; b) E. Doblhofer, A. Heidebrecht, T. Scheibel, *Appl. Microbiol. Biotechnol.* **2015**, *99*, 9361 – 9380; c) M. Heim, D. Keerl, T. Scheibel, *Angew. Chem. Int. Ed.* **2009**, *48*, 3584 – 3596; *Angew. Chem.* **2009**, *121*, 3638 – 3650.
[13] D. R. Canchi, A. E. García, *Annu. Rev. Phys. Chem.* **2013**, *64*, 273 – 293.
[14] C. N. Pace, S. Treviño, E. Prabhakaran, J. M. Scholtz, *Philos. Trans. R. Soc. London Ser. B* **2004**, *359*, 1225 – 1235.
[15] N. Javid, K. Vogtt, C. Krywka, M. Tolan, R. Winter, *ChemPhysChem* **2007**, *8*, 679 – 689.
[16] A. Lammel, M. Schwab, U. Slotta, G. Winter, T. Scheibel, *ChemSusChem* **2008**, *1*, 413 – 416.
[17] E. Doblhofer, T. Scheibel, *J. Pharm. Sci.* **2015**, *104*, 988 – 994.
[18] a) S. Kumari, G. Lang, E. DeSimone, C. Spengler, V. T. Trossmann, S. Lücker, M. Hudel, K. Jacobs, N. Krämer, T. Scheibel, *Data Brief* **2020**, *32*, 106305; b) S. Kumari, G. Lang, E. DeSimone, C. Spengler, V. T. Trossmann, S. Lücker, M. Hudel, K. Jacobs, N. Krämer, T. Scheibel, *Mater. Today* **2020**, *41*, 21 – 33.
[19] M. R. Harpham, N. E. Levinger, B. M. Ladanyi, *J. Phys. Chem. B* **2008**, *112*, 283 – 293.
[20] H. M. Herold, A. Döbl, S. Wohlrab, M. Humenik, T. Scheibel, *Biomacromolecules* **2020**, *21*, 4904 – 4912.
[21] K. D. Hermanson, D. Huemmerich, T. Scheibel, A. R. Bausch, *Adv. Mater.* **2007**, *19*, 1810 – 1815.
[22] K. D. Hermanson, M. B. Harasim, T. Scheibel, A. R. Bausch, *Phys. Chem. Chem. Phys.* **2007**, *9*, 6442 – 6446.
[23] J. Hansen, F. Platten, D. Wagner, S. U. Egelhaaf, *Phys. Chem. Chem. Phys.* **2016**, *18*, 10270 – 10280.
[24] D. N. Shin, J. W. Wijnen, J. B. F. N. Engberts, A. Wakisaka, *J. Phys. Chem. B* **2002**, *106*, 6014 – 6020.
[25] a) S. Roy, S. Banerjee, N. Biyani, B. Jana, B. Bagchi, *J. Phys. Chem. B* **2011**, *115*, 685 – 692; b) A. Wakisaka, H. Abdoul-Carime, Y. Yamamoto, Y. Kiyozumi, *J. Chem. Soc. Faraday Trans.* **1998**, *94*, 369 – 374; c) A. Wakisaka, T. Ohki, *Faraday Discuss.* **2005**, *129*, 231 – 245; d) D. B. Wong, K. P. Sokolowsky, M. I. El-Barghouthi, E. E. Fenn, C. H. Giammanco, A. L. Sturlaugson, M. D. Fayer, *J. Phys. Chem. B* **2012**, *116*, 5479 – 5490.
[26] C. B. Borkner, S. Lentz, M. Müller, A. Fery, T. Scheibel, *ACS Appl. Polym. Mater.* **2019**, *1*, 3366 – 3374.
[27] K. L. Shaw, G. R. Grimsley, G. I. Yakovlev, A. A. Makarov, C. N. Pace, *Protein Sci.* **2001**, *10*, 1206 – 1215.
[28] K. Capriotti, J. A. Capriotti, *J. Clin. Aesthet. Dermatol.* **2012**, *5*, 24 – 26.
[29] J. Petzold, T. B. Aigner, F. Touska, K. Zimmermann, T. Scheibel, F. B. Engel, *Adv. Funct. Mater.* **2017**, *27*, 1701427.
[30] X. Hu, D. Kaplan, P. Cebe, *Macromolecules* **2006**, *39*, 6161 – 6170.

Manuscript received: March 3, 2021
Accepted manuscript online: March 26, 2021
Version of record online: May 1, 2021

